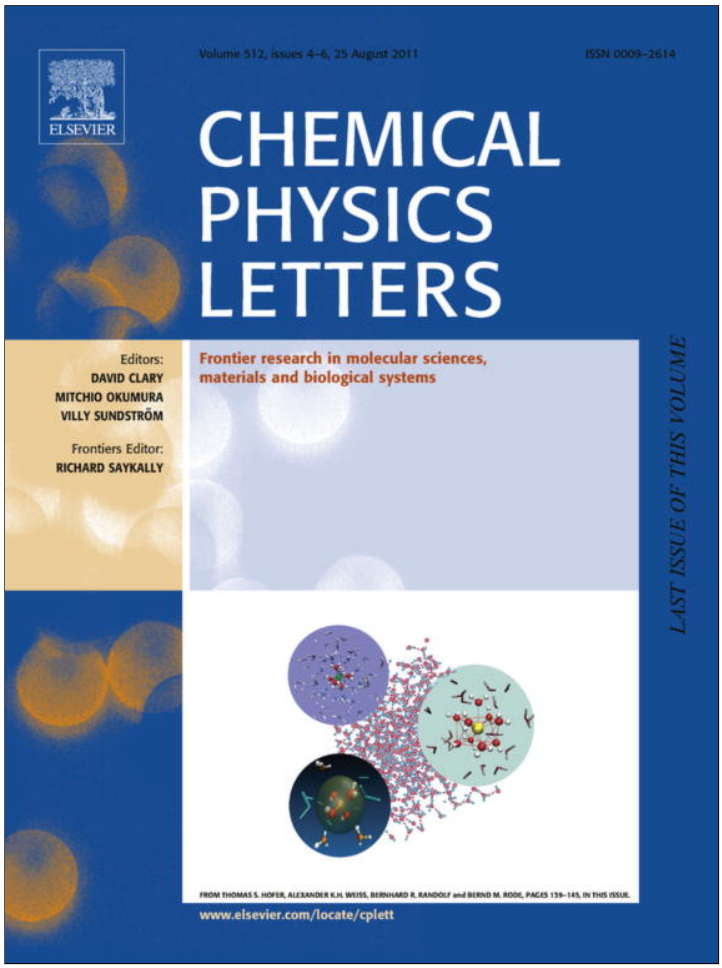

Chemical Physics Letters 512 (2011) 243–246

Contents lists available at ScienceDirect

Chemical Physics Letters

journal homepage: www.elsevier.com/locate/cplett

Structure–property relationships for methyl-terminated alkyl self-assembled monolayers

Frank W. DelRio [a,*], David M. Rampulla [b], Cherno Jaye [a], Gheorghe Stan [a], Richard S. Gates [a], Daniel A. Fischer [a], Robert F. Cook [a]

[a] Ceramics Division, Material Measurement Laboratory, National Institute of Standards and Technology, Gaithersburg, MD 20899, USA
[b] Surface and Microanalysis Science Division, Material Measurement Laboratory, National Institute of Standards and Technology, Gaithersburg, MD 20899, USA

ARTICLE INFO

Article history:
Received 23 May 2011
In final form 13 July 2011
Available online 20 July 2011

ABSTRACT

Structure–property relationships for methyl-terminated alkyl self-assembled monolayers (SAMs) are developed using near-edge X-ray absorption fine structure (NEXAFS) spectroscopy and atomic force microscopy (AFM). NEXAFS C *K*-edge spectra are used to compute the dichroic ratio, which provides a quantitative measure of the molecular structure. AFM data are analyzed with an elastic adhesive contact model, modified by a first-order elastic perturbation method to include substrate effects, to extract the monolayer mechanical properties. Using this approach, the measured mechanical properties are not influenced by the substrate, which allows universal structure–property relationships to be developed for methyl-terminated alkyl SAMs.

Published by Elsevier B.V.

1. Introduction

The organization of self-assembled monolayers (SAMs) onto solid surfaces has received significant attention for both technological and fundamental reasons [1]. Not only do SAMs show great potential as protective layers to slow oxidation [2], photoresistive layers for lithography [3], electrically-switchable layers to alter wettability [4], and interfacial lubrication layers to mitigate adhesion and friction [5], but they also provide excellent model systems for understanding the nano-scale mechanisms behind macro-scale phenomena such as corrosion, wetting, and lubrication [6]. SAMs are useful in so many different applications because of their versatile structure–property relationships; the head group (which connects the SAM to the solid surface), tail group (which represents the outer surface of the SAM), and spacer chain (which forms the backbone of the SAM) can be tailored to achieve a nearly unlimited array of binding energies, adhesion energies, and Young's moduli, respectively [7]. To take advantage of this versatility, it is necessary to understand the function of each building block and how it influences the overall structure–property relationships *and* elucidate the mechanisms responsible for each relationship. For example, in a previous study [8], the length of the spacer chain was shown to determine the Young's moduli, which were then used to reveal universal behavior of the electrical properties and a single mechanism for collapse under contact. In this Letter, we examine the role of the *head group* on molecular structure and mechanical properties via a comparative study of two methyl-terminated alkyl SAMs: alkylthiols ($CH_3(CH_2)_{n-1}SH$) on Au and alkylphosphonates ($CH_3(CH_2)_{n-1}PO(OH)_2$) on indium tin oxide (ITO), denoted as C_n, where n is the number of carbons in the spacer chain. Near-edge X-ray absorption fine structure (NEXAFS) data provide a quantitative measure of monolayer structure and atomic force microscopy (AFM) data are analyzed to extract monolayer mechanical properties. As with previous work [8,9], a critical factor in developing SAM structure–property relationships is the use of a method that takes substrate properties into account, thus generating SAM properties that are not artificially inflated.

2. Experimental

Si(1 0 0) substrates were coated with a 5 nm Ti adhesion layer followed by a 100 nm Au film. The Au-coated Si samples were cleaned with acetone, isopropyl alcohol, and ultraviolet ozone; immersed in 1 mM ethanolic solutions of the thiols (n = 5, 8, 12, and 18) for 24 h; rinsed in ethanol; and dried with N_2. Alkali-earth boroaluminosilicate glass substrates were coated with a 150 nm ITO film. The ITO-coated glass samples were cleaned with acetone, isopropyl alcohol, and ultraviolet ozone; immersed in 1 mM anhydrous tetrahydrofuran solutions of the phosphonates (n = 8, 10, 12, and 18) for 24 h; rinsed in tetrahydrofuran; and dried with N_2. The samples were stored in a class 100 cleanroom for at least a week to allow for monolayer diffusion and ripening [10]. AFM experiments were performed in ambient conditions (21 °C, 45% relative humidity) with Si cantilevers coated with 60 nm of Co followed by 20 nm of Cr. The cantilever spring constants in the normal direction, k, were determined by laser Doppler vibrometry [11]; values for k varied between 0.9 and 1.4 N m^{-1}. The probe tips were character-

* Corresponding author.
E-mail address: frank.delrio@nist.gov (F.W. DelRio).

0009-2614/$ - see front matter Published by Elsevier B.V.
doi:10.1016/j.cplett.2011.07.045

ized before and after the contact experiments to check for damage by imaging microfabricated Si spikes. The radius R of the highest protrusion, or asperity, was ≈20 nm, with no discernable changes due to contact. Force–deformation (F–δ) data were derived from force–displacement (F–d) curves by subtracting cantilever deflection, F/k. Only the unloading portion of each F–d curve was considered, as the displacements are elastic, allowing the data to be interpreted via elastic contact theory. The maximum F was ≈15 nN, which translates to contact pressures below those required to induce lateral displacement of alkyl SAMs [12]. NEXAFS measurements were carried out at the NIST U7A beamline of the National Synchrotron Light Source. Partial electron yield (PEY) spectra at the C K-edge were obtained with a channeltron retarding voltage of −225 V to enhance surface sensitivity and Auger yield. NEXAFS spectra were taken at angles, θ, ranging from 20° to 90°, measured between the sample surface and the photon beam.

3. Results and discussion

AFM F–δ data for the thiols and phosphonates are shown in Figure 1a and b, respectively. Young's modulus, E_{film}, and work of adhesion, w, of the film can be extracted from the F–δ curves with the Derjaguin–Muller–Toporov (DMT) contact model, an elastic theory that includes adhesive forces in the response of a sphere with radius R against a flat surface [13].

$$F = \frac{4}{3}E^* R^{1/2}\delta^{3/2} - 2\pi R w \tag{1}$$

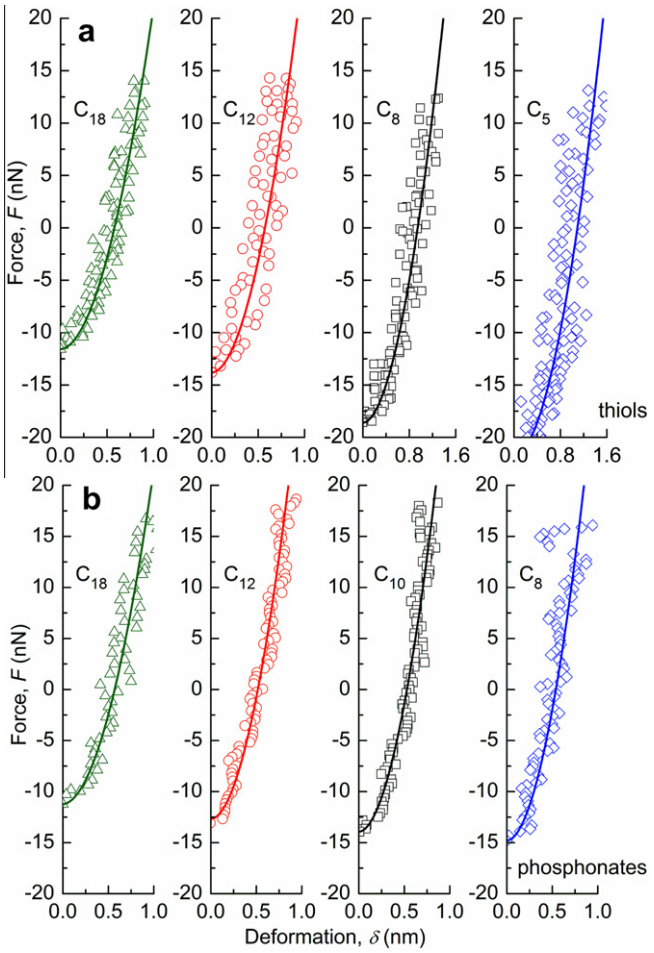

Figure 1. AFM F–δ data (symbols) and theoretical fits (solid lines) for (a) thiols on Au and (b) phosphonates on ITO.

where E^* is the reduced modulus of the contact. Xu and Pharr developed an analytical solution for E^* of a film on substrate system, which considered Young's moduli and Poisson's ratios of the film (E_{film}, ν_{film}) *and* substrate (E_{sub}, ν_{sub}). In the model, E^* is given by [14]

$$\frac{1}{E^*} = \frac{1}{2}[1 - \nu_{sub} + (\nu_{sub} - \nu_{film})I_1]\left[\frac{2(1+\nu_{sub})}{E_{sub}}(1 - I_0) + \frac{2(1+\nu_{film})}{E_{film}}I_0\right] \tag{2}$$

where I_0 and I_1 are weighting functions that account for shear modulus mismatch and Poisson's ratio effects, respectively. E_{sub} = 77 GPa and ν_{sub} = 0.42 were used for Au [15], E_{sub} = 88 GPa and ν_{sub} = 0.33 were used for ITO [16], and ν_{film} = 0.44 was used for alkyl SAMs [17]. To find w, Eq. (1) was solved at δ = 0, which results in $w = -F_{po}/2\pi R$, where F_{po} is the pull-off force from each F–δ data set. To find E_{film}, Eqs. (1) and (2) were fit to the full F–δ curves as shown in Figure 1. The values for w and E_{film} are given in Table 1. Using these values, the probe tip radius, and the equilibrium separations from Figure 1, the Tabor parameter [18] was found to be $\mu \approx 0.3$ (at F = 0) for all monolayers, justifying the use of the DMT model. As F increases, E^* increases (due to substrate effects) and μ decreases, pushing the system further into the DMT zone.

Figure 2 is a plot of w and E_{film} as a function of n. For the thiols, the values for w and E_{film} are within uncertainty of results from ultra-high vacuum studies [8,9], suggesting that capillary meniscus forces were negligible here, consistent with previous work on capillary interactions with hydrophobic SAMs [19]. Therefore, w and E_{film} can be described by van der Waals interactions at the tip-monolayer and tip-substrate interfaces and between the alkyl chains, respectively. From this observation, it is possible to partially explain the overall trends in Figure 2, namely the monotonic increase in w and decrease in E_{film} as n decreases, in terms of variations in the van der Waals interactions with n. As n decreases, the stabilization energy between alkyl chains decreases, which reduces the film's resistance to elastic deformation (i.e., decreases E_{film}), thereby exposing the tip to additional functional groups in the film or to the substrate (i.e., increases w). However, it is evident that n does not solely determine the monolayer mechanical properties, as alkyl SAMs with similar n, but different head groups, sometimes exhibited drastically different values for w and E_{film} (e.g., see n = 8 in Figure 2). As a result, to develop structure–property relationships, a structural metric that not only considers the spacer chain, but also the role of the head group and tail group, is needed and is considered in the next section.

NEXAFS C K-edge PEY spectra for the thiols and phosphonates are shown in Figure 3a and b, respectively. All spectra exhibit the same hydrocarbon resonance peaks: the C=C π^* peak at 285.5 eV, the C—H σ^* peak at 288.6 eV, and the C—C σ^* peak at 293.6 eV. In Figure 3a, the spectra exhibit a strong angular dependence for n = 18 and 12, but are nearly identical for n = 8 and 5. In addition, as n decreases, the intensity of the C=C π^* resonance

Table 1
w, E_{film}, and C—H σ^* R_l for thiols on Au and phosphonates on ITO.

n	Head group	w (mJ m^{-2})[a]	E_{film} (GPa)[a]	C—H σ^* R_l[b]
5	Thiol	166.9 ± 21.3	0.12 ± 0.03	0.04 ± 0.04
8	Thiol	147.7 ± 16.0	0.26 ± 0.03	0.02 ± 0.02
	Phosphonate	117.4 ± 10.3	0.67 ± 0.09	0.20 ± 0.03
10	Phosphonate	113.1 ± 12.4	0.72 ± 0.06	0.23 ± 0.03
12	Thiol	110.9 ± 7.8	0.80 ± 0.09	0.26 ± 0.02
	Phosphonate	102.1 ± 4.3	0.89 ± 0.09	0.33 ± 0.01
18	Thiol	92.6 ± 8.9	0.97 ± 0.13	0.50 ± 0.03
	Phosphonate	93.2 ± 4.3	0.96 ± 0.06	0.46 ± 0.01

[a] Uncertainty values represent two standard deviations from at least 10 measurements or;
[b] A 95% confidence level in the fit.

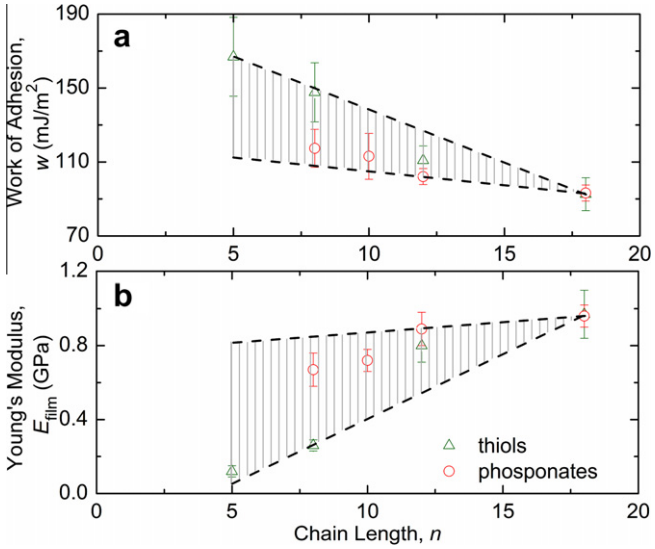

Figure 2. (a) w and (b) E_{film} as a function of n for thiols on Au and phosphonates on ITO. Uncertainty values represent two standard deviations from at least 10 measurements. Lines are a guide to the eyes.

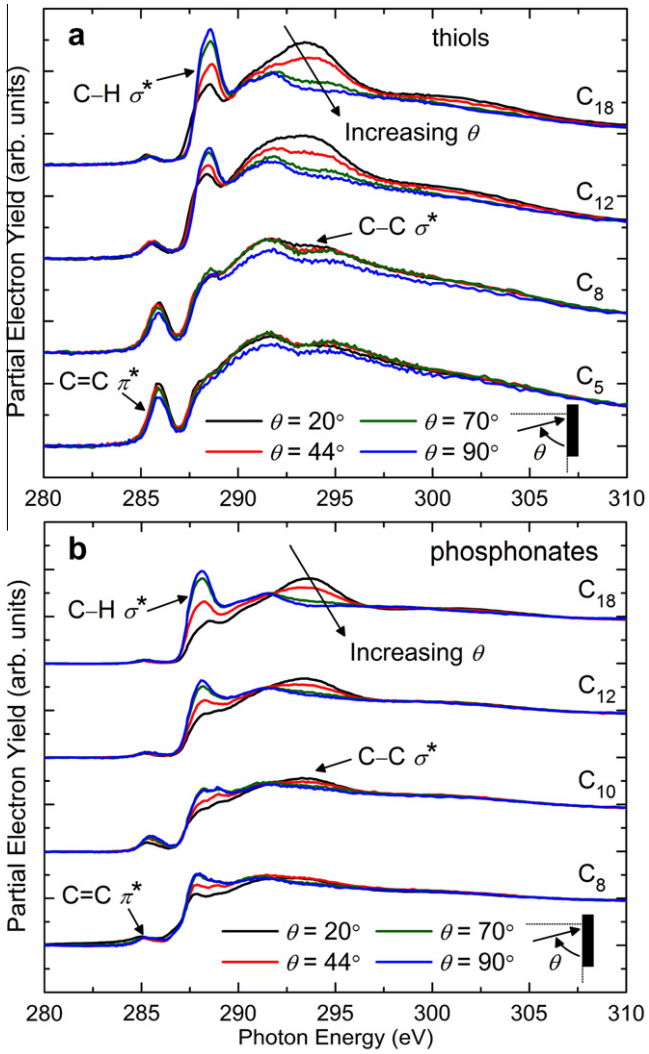

Figure 3. NEXAFS C K-edge PEY spectra for (a) thiols on Au and (b) phosphonates on ITO at $\theta = 20°$, 44°, 70°, and 90°.

peak, which is associated with adventitious hydrocarbons, increases. In Figure 3b, the spectra exhibit angular dependence for all n, with a decrease in dependence as n decreases, and the intensity of the C=C π^* peak is small and invariant with n. The variations in peak intensity with θ can be quantitatively related to molecular orientation through the dichroic ratio, $R_l = (I_{90°} - I_{0°})/(I_{90°} + I_{0°})$, where $I_{90°}$ is the peak intensity at $\theta = 90°$ and $I_{0°}$ is the peak intensity at $\theta = 0°$. R_l can vary from -1 to +0.75, with a more positive value for the C—H σ^* peak corresponding to greater surface normality and monolayer crystallinity ($R_l = 0$ may represent a random distribution of chain orientations) [20]. Table 1 summarizes the C—H σ^* dichroic ratios. For both the thiols and phosphonates, R_l decreases as n decreases, which points to a structural dependence on n, consistent with the observations from Figure 2. Furthermore, from the R_l results, it is clear that the change in phase from crystalline to amorphous occurs at different n ($8 < n < 12$ for the thiols and $n < 8$ for the phosphonates), which explains the different values for w and E_{film} at $n = 8$ in Figure 2. Thus, R_l is sensitive to changes in both the spacer chain and the head group.

Figure 4 is a plot of w and E_{film} as a function of R_l; universal behavior is observed for both properties as a function of this structural measure, and the trends can be divided into three regions. In region 1, the properties do not change as R_l decreases, implying that although there is a change in chain orientation, the gross SAM structural features (i.e., SAM termination by CH_3 groups and chain–chain interactions) remain largely unaltered. In region 2, the gross structure of the film is gradually altered as R_l decreases, as chain–chain SAM stabilization forces decrease with increasing tilt angle and *gauche* defects form in the topmost methyl units [21], leading to a monolayer with densely-packed *and* amorphous regions. The exposure of the probe tip to CH_2 groups and the substrate leads to an increase in w and the decrease in chain–chain stabilization leads to a decrease in E_{film}. In region 3, the monolayer is completely amorphous and there is significant thermal desorption of the alkyl chains. Such desorption processes continue until a coverage-dependent heat of adsorption makes the film stable, as with the short-chain thiols here, or to completion [22]. The desorbed chains are replaced with adventitious hydrocarbons, evident from the C=C π^* peaks in Figure 3a. Thus, w and E_{film} are due to the remaining alkyl chains *and* the adventitious hydrocarbons, with w and E_{film} ultimately converging to those for a full adventitious hydrocarbon layer. The phosphonates are less prone to desorption

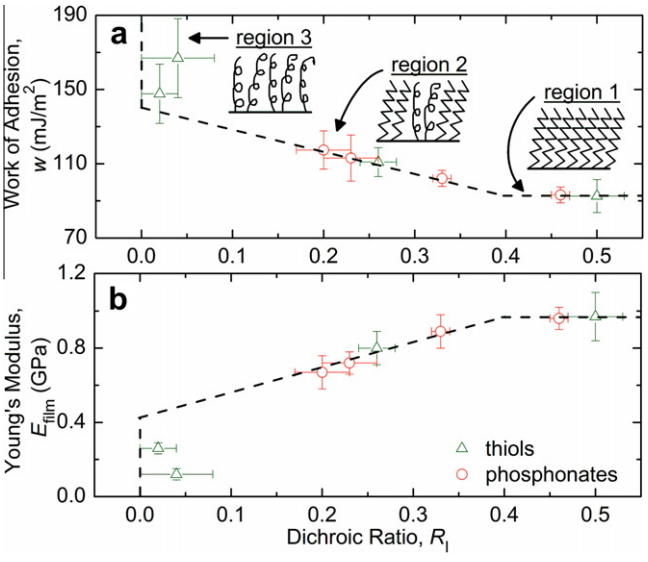

Figure 4. (a) w and (b) E_{film} as a function of R_l for thiols on Au and phosphonates on ITO. Uncertainty values represent two standard deviations from at least 10 measurements or a 95% confidence level in the fit. Lines are a guide to the eyes.

due to the bidentate/tridentate binding configurations to ITO [23], in contrast to the thiols, which exhibit monodentate binding to Au.

4. Summary and conclusions

In summary, mechanical properties of methyl-terminated alkyl SAMs were examined with AFM and correlated with surface structure via NEXAFS. The structure–property relationships appear to be universal for methyl-terminated alkyl SAMs only when plotted in terms of R_l, as the thiol and phosphonate data fall onto the same curves, despite differences in head group. R_l is a more complete structural measure, as it not only considers variations in the spacer chain, but also the role of the head group and tail group. Further work on SAMs with different head groups, tail groups, and spacer chains will allow similar structure–property trends to be established.

References

[1] A. Ulman, Chem. Rev. 96 (1996) 1533.
[2] P.E. Laibinis, G.M. Whitesides, J. Am. Chem. Soc. 114 (1992) 9022.
[3] V.C. Sundar, J. Aizerberg, Appl. Phys. Lett. 83 (2003) 2259.
[4] J. Lahann et al., Science 299 (2003) 371.
[5] R. Maboudian, R.T. Howe, J. Vac. Sci. Technol. B 15 (1997) 1.
[6] D.K. Schwartz, Annu. Rev. Phys. Chem. 52 (2001) 107.
[7] B. Bhushan, H. Liu, Phys. Rev. B 63 (2001) 245412.
[8] F.W. DelRio, K.L. Steffens, C. Jaye, D.A. Fischer, R.F. Cook, Langmuir 26 (2010) 1688.
[9] F.W. DelRio, C. Jaye, D.A. Fischer, R.F. Cook, Appl. Phys. Lett. 94 (2009) 131909.
[10] E. Barrena, C. Ocal, M. Salmeron, J. Chem. Phys. 111 (1999) 9797.
[11] B. Ohler, Rev. Sci. Instrum. 78 (2007) 063701.
[12] G. Liu, M.B. Salmeron, Langmuir 10 (1994) 367.
[13] B.V. Derjaguin, V.M. Muller, Y.P. Toporov, J. Colloid Interface Sci. 53 (1975) 314.
[14] H. Xu, G.M. Pharr, Scripta Mater. 55 (2006) 315.
[15] W.D. Callister, Materials Science and Engineering: An Introduction, John Wiley and Sons, New York, 2000.
[16] T. Wittkowski, J. Jorzick, H. Seitz, B. Schröder, K. Jung, B. Hillebrands, Thin Solid Films 398–399 (2001) 465.
[17] M. Wang, K.M. Liechti, V. Srinivasan, J.M. White, P.J. Rossky, M.T. Stone, J. Appl. Mech. 73 (2006) 769.
[18] D. Tabor, J. Colloid Interface Sci. 58 (1977) 2.
[19] M. Binggeli, C.M. Mate, J. Vac. Sci. Technol. B 13 (1995) 1312.
[20] S. Sambasivan, S. Hsieh, D.A. Fischer, S.M. Hsu, J. Vac. Sci. Technol. A 24 (2006) 1484.
[21] J. Hautman, M.L. Klein, J. Chem. Phys. 91 (1989) 4994.
[22] R.G. Nuzzo, B.R. Zegarski, L.H. Dubois, J. Am. Chem. Soc. 109 (1987) 733.
[23] P.B. Paramonov, S.A. Paniagua, P.J. Hotchkiss, S.C. Jones, N.R. Armstrong, S.R. Marder, J.-L. Brédas, Chem. Mater. 20 (2008) 5131.